A Framework for the Design of a Magnet-Based Multistable Rotational Stage

van Noordt, Thijs; t'Sas, Justus; Verzijl, Nikai; Wong, Luka; Herder, Just L.; Roberjot, Pierre

DOI
10.1115/DETC2025-167855

Publication date
2025

Document Version
Final published version

Published in
Proceedings of the 21st IEEE/ASME International Conference on Mechatronic and Embedded Systems and Applications (MESA); 49th Mechanisms and Robotics Conference (MR)

Citation (APA)
van Noordt, T., t'Sas, J., Verzijl, N., Wong, L., Herder, J. L., & Roberjot, P. (2025). A Framework for the Design of a Magnet-Based Multistable Rotational Stage. In *Proceedings of the 21st IEEE/ASME International Conference on Mechatronic and Embedded Systems and Applications (MESA); 49th Mechanisms and Robotics Conference (MR)* (Vol. 5). Article v005t08a053 American Society of Mechanical Engineers (ASME). https://doi.org/10.1115/DETC2025-167855

Proceedings of the ASME 2025
International Design Engineering Technical Conferences and
Computers and Information in Engineering Conference
IDETC-CIE2025
August 17-20, 2025, Anaheim, CA

DETC2025-167855

A FRAMEWORK FOR THE DESIGN OF A MAGNET-BASED MULTISTABLE ROTATIONAL STAGE

Thijs van Noordt [1,†], Justus t'Sas[1,†], Nikai Verzijl[1,†], Luka Wong [1,†], Just L. Herder[1,*], Pierre Roberjot[1,*]

[1]Department of Precision and Microsystems Engineering, Delft University of Technology , Delft 2628 CD , The Netherlands

ABSTRACT

Multistable metamaterials are architected structures capable of adopting multiple stable geometrical configurations. This unique characteristic makes them highly valuable for stiffness control, energy harvesting, and morphing technologies. As a result, multistable structures hold great potential for diverse applications across various fields.

The development of multistable metamaterials primarily relies on buckled beam technology, enabling the creation of a wide range of structures. However, only a few rotational multistable designs have been explored. Additionally, the geometry of buckled beams imposes constraints on the range of motion.

To overcome these limitations, our work introduces a novel design method for magnet-based rotational multistable stages. This approach, grounded in the electrostatic ideal dipole assumption, enables precise control over the angle of multistability and the stiffness of the stable states.

Keywords: Bistability, multistability, negative stiffness, magnets, rotational stage, design method

1. INTRODUCTION

Reconfigurable multistable structures have gained increasing popularity in both academic and commercial fields due to their ability to harness spatial deformation and enable controlled stiffness behavior. Advancements in multistable structures will further drive the development of morphing technologies [1], compliant and soft robotics [2, 3], and energy harvesters [4, 5]. Buckled beams, derived from Von Mises trusses [6, 7], are compliant bistable structures that exhibit snap-through behavior. Bistability is characterized by a negative slope in the force-displacement relationship, with a minimum force occurring below the point of force application [8]. This phenomenon is commonly referred to as negative stiffness behavior. Buckled beams can be fabricated using two approaches [9]. In the first method, a straight beam is manufactured and then laterally loaded to induce buckling, resulting in two stable positions with symmetric buckling energy. In the second method, the beam is pre-shaped in a buckled configuration, still allowing for buckling but introducing energy asymmetry between the two stable states.

Multistability can be achieved by combining bistable structures [10, 11], enabling discrete deformation, tailored multistiffness behavior, and specific deformation patterns. Bistable beams are commonly used in the design of unidirectional linear multistable structures. However, spatial configurations and modifications can introduce additional modes of bistability, such as tilting bistability [3, 12, 13]. Beyond tilt-based multistability, rotational bistability can also be realized using bistable beams. In this approach, one end of the bistable beam is attached to an inner rotating frame, while the other end is connected to an outer frame [14]. This configuration results in rotational bistability. Furthermore, rotational multistability can be achieved by concentrically combining multiple rotational bistable structures [15].

Despite their promising potential, buckled-beam-based multistable structures are limited in their range of motion. While buckled beams enable bistability, their geometry also restricts movement. Bistability arises due to the stress field in the beams, which acts as a repulsive force between the connection points and the beam's midpoint in bistable linear structures. In rotational bistability, this repulsive interaction occurs between the two edges of the beam. Consequently, incorporating repulsive elements within a force field could enable the design of bi- and multistable structures with an extended range of motion. The repulsive magnetic field generated by magnets has been explored as a means to replicate the bistable behavior of buckled beams [16, 17]. Following this principle, rotational multistability can also be achieved using magnetic fields. A similar approach is already employed in permanent magnet motors, which utilize both permanent magnets and electromagnets. Magnet-based rotational multistable structures hold significant potential for fundamental advancements, paving the way for improved positioning

[†]Joint first authors
[*]Corresponding author: P.Roberjot@tudelft.nl
Documentation for `asmeconf.cls`: Version 1.38, May 17, 2025.

stages, manipulators, and energy harvesters.

In this paper, we first introduce a design framework for magnet-based multistable rotating stages, leveraging an electrostatic assumption with ideal dipoles. This approach establishes the ideal torque-angle relationship between a fixed dipole and a moving dipole rotating along a circular path around a center of rotation, considering both attractive and repulsive configurations. Next, we generalize the torque-angle equations for any number of concentric rings, each containing an arbitrary number of dipoles. Based on this, we propose a design method that enables the creation of multistable stages with a desired number of stable positions and tunable stiffness. Finally, we apply our design method to develop a magnet-based multistable rotational stage with a specific stable angle. The performance of the design is validated through finite element analysis and experimental testing.

2. METHODS

In this section, we first present the two bases of magnet-based bistable structures, second, we propose a design framework for multi-ring rotational multistable magnet-based stage, then we detail the materials used for fabrication, the design of the set up and detail the finite element model (FEM) for characterizing the structure.

2.1 Magnet configurations

Planar bistable structures can have two motion types. The first and most common is the linear motion where a base possesses a discrete linear motion relative to a base. In this case, one magnet is attached to the ground and a second is on rollers and able to roll on a plane parallel to the ground. This scenario is identical to having the second magnet attached to an arm of infinite length L_L fixed to a revolute joint fixed to the ground, illustrated in **Figure 1.a**.

The second, the rotational bistable motion is composed of a magnet fixed to the ground and, a second one attached to an arm of finite length L_R linked to a revolute joint O_R fixed to the ground, illustrated in **Figure 1.b**.

For these two types of motion exists six configurations of the magnets illustrated in **Figure 1.c.d**. The first three are based on the repulsion of the two magnets [17], the magnets are thus at unstable equilibrium when facing and, at stable equilibrium when they are far enough, at a distance d sufficient for the magnetic forces to be negligible. Three configurations are possible:

1. The two magnets have both their their south (respectively north) poles facing each other,
2. The two magnets are facing each other as in 1. and are rotated with an angle $\pm\theta$,
3. The two magnets are facing sideways, where the north (respectively south) pole of the first faces the south (respectively north) pole of the second, in this case $\theta = \pm 90°$

To obtain bistability with the repulsive configurations there is need of at least three magnets. One is able to move and the two others, of opposite charge, are fixed on a line for linear bistability and, on a circle for rotational bistability. Assuming the magnets possess the same charge, the stable equilibrium point is located at the point between and equidistant to the the two fixed magnets.

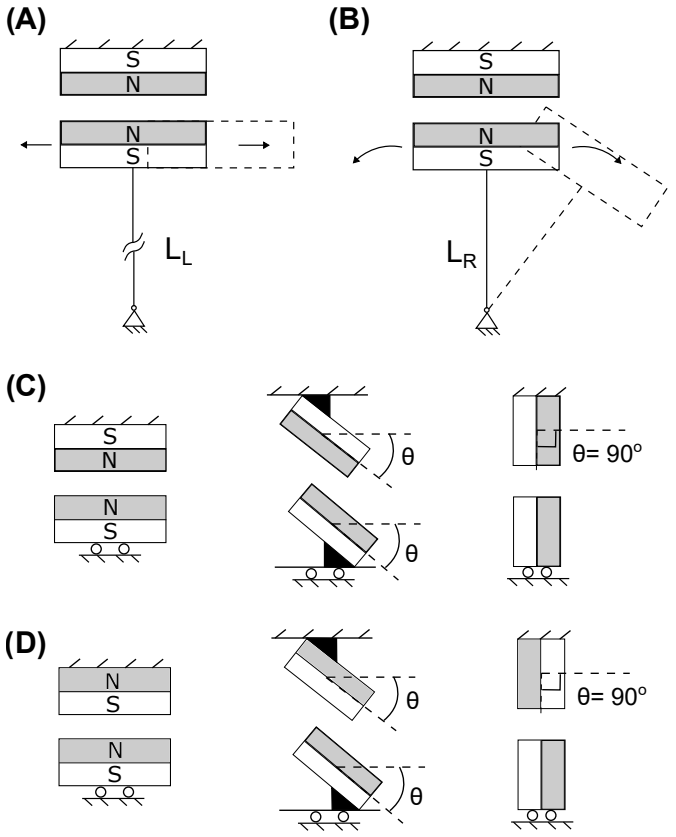

FIGURE 1: REPRESENTATION OF (A) THE BISTABLE LINEAR MOTION, (B) THE BISTABLE ROTATIONAL MOTION, (C) THE THREE REPULSIVE CONFIGURATIONS AND, (D) THE THREE ATTRACTIVE CONFIGURATIONS, BOTH FOR LINEAR AND ROTATIONAL MOTION.

The last three are the same as presented above but using the attraction between two magnets. The magnets are at stable equilibrium when the distance d is minimal, thus when they are facing. Whereas, the unstable equilibrium is when the magnets are at a distance d sufficient for the magnetic forces to be negligible. Bistability is also present for, at least, a three-magnet configuration. One magnet is able to move and faces a fixed magnet n, if subjected to a sufficient force or torque, the magnet will tend to align with the magnet $n+1$ forming a bistable unit.

2.2 Ideal dipole-based bistability

Here we are proposing the design of magnet-based multistable stages with the assumption of ideal dipoles. First, we propose the theory for linear multistable motion. Second, we extend this theory to rotational multistability motion.

2.2.1 Bistable linear motion. Linear bistable motions are characterized by their force-displacement relation, whereas the rotational bistable motion are characterized by their torque-angle relation.

Where the force between two ideal magnetic dipoles (where the dipole is the center of the magnet), where one is fixed A and,

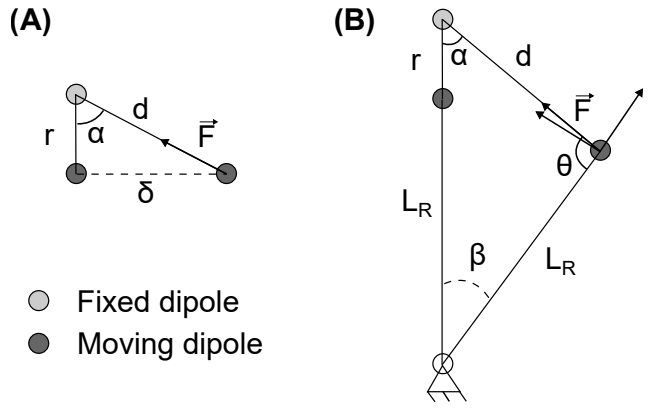

FIGURE 2: REPRESENTATION OF (A) THE LINEAR MOTION AND, (B) THE ROTATING MOTION OF TWO DIPOLES.

the second X is able to move on a line, could be described with Coulomb's law, the force potential F is written

$$F(d) = \frac{k_e q_i q_j}{d^2} \tag{1}$$

with k_e the Coulomb's constant ($k_e = 8.987551.10^9 N.m^2.C^{-2}$), q_i and q_j the charges of the two dipoles ($q_i = q_j$ for repulsive and, $q_i = -q_j$ for attractive dipoles of same charges) we will assume charges of $q = 10^{-9}$ C, d is the distance between the dipoles. In the case of a linear motion (**Figure 2.A**), if a displacement δ is applied to the moving magnet, the distance d between the two dipoles becomes

$$d = \sqrt{r^2 + \delta^2} \tag{2}$$

with r the initial value of the distance d. Therefore the dipole force-displacement relation can be written as

$$F(\delta) = \frac{k_e q_i q_j}{r^2 + \delta^2} \cos(\alpha) \tag{3}$$

with

$$\cos(\alpha) = \frac{r}{d} \tag{4}$$

As stated in **Section 2.1**, at least three dipoles are needed to obtain bistability, considering a system of two fixed dipoles separated by a distance D and, one moving (equivalent to two dipoles moving and one fixed), the resulting Coulomb force ($F_C(\delta)$) between the dipoles becomes

$$F_C(\delta) = F(\delta) + F(D - \delta) \tag{5}$$

with $\delta \in [0, D]$. The Coulomb force $F_C(\delta)$ is minimal for repulsive dipoles (respectively maximal for attractive dipoles) at $\delta = D/2$, and maximal at $\delta = \{0, D\}$ (respectively minimal).

2.2.2 Bistable rotational motion. A similar approach could be used for the rotation motion of dipoles (**Figure 2.B**) described by their torque-angle relation. A first dipole is fixed at a distance $L_R + r$ and, a second is attached to a rotating arm of length L_R, the two dipoles are facing each other with a distance $d = r$. The force $\mathbf{F}(d)$ between two dipoles is described by **Equation 1** where, when an angular displacement β is applied to the moving dipole the distance $d(\beta)$ between the dipoles changes, and can be derived with the Al-Kashi formula as

$$d^2(\beta) = (L_R + r)^2 + L_R^2 - 2L_R(L_R + r)\cos(\beta) \tag{6}$$

Only the normal component of the force contributes to the torque on the moment arm L_R, the magnitude of the torque can thus be written

$$T(\beta) = F(\beta) L_R \sin(\theta) \tag{7}$$

the law of sinuses gives

$$\frac{\sin(\beta)}{d(\beta)} = \frac{\sin(\theta)}{(L_R + r)} \tag{8}$$

thus $\sin(\theta)$ can be replaced in **Equation 7**

$$T(\beta) = F(\beta) L_R \frac{\sin(\beta)(L_R + r)}{d(\beta)} \tag{9}$$

Therefore, the dipole torque-angle relation can be written as

$$T(\beta, L_R, r) = \frac{Q L_R (L_R + r)\sin(\beta)}{d^3(\beta)} \tag{10}$$

with $Q = k_e q_i q_j$ and for simplification $Q = -1.10^{-9} N.m^2$ for attractive dipoles and $Q = 1.10^{-8} N.m^2$ for repulsive dipoles. The rotational stiffness $\kappa(\beta, L_R, r)$ is the derivative of the torque $T(\beta, L_R, r)$ presented in **Appendix A**

$$\kappa(\beta, L_R, r) = \frac{dT(\beta, L_R, r)}{d\beta} \tag{11}$$

Three dipoles are required to obtain bistability, therefore the minimal configuration is (1.2), representing the two rings, the inner ring possessing 1 dipole and the second 2 dipoles. The configurations where only one dipole is in interaction with a ring possessing N dipoles is denoted $(1.N)$. $(1.N)$ possesses N stable positions and is making an bistable angle $\varphi_N = \frac{360°}{N}$. The resulting torque $T_C(\beta, N, L_R, r)$ between the dipoles, similarly to **Equation.5**, becomes

$$T_C(\beta, N, L_R, r) = T(\beta, L_R, r) + T(\varphi_N - \beta, L_R, r) \tag{12}$$

with $\beta \in [0, \varphi_N]$. The torque is minimal for repulsive dipoles (respectively maximal for attractive dipoles) for $\beta = \varphi_N/2$ and, maximal (respectively minimal) at $\beta = \{0, \varphi_N\}$.

Similar to the linear motion bistability, in the case of a uniform distribution of dipoles on the fixed circle, **Equation 12** holds true assuming periodic boundary conditions. The contribution of the dipoles away from dipoles n and $n+1$ (where the moving dipole is able to move) are considered negligible, however, it is possible to write the total contribution of a configuration (1.N), of dimensions L_R and r, from **Equation 10** as

$$T_N(\beta, L_R, r) = \sum_{i=0}^{N-1} T(i\varphi_N - \beta, L_R, r) \tag{13}$$

In a (n_1, n_2) configuration, the torque-angle relation becomes the contribution of all the dipoles in the system. The torque-angle

relation could be written as a more general case, from **Equation 13**, as

$$T(\beta, n_1, n_2, L_R, r) = c \sum_{j=0}^{n_m-1} \sum_{i=0}^{n_{max}-1} T\left(i\varphi_m - \beta - j\varphi, L_R, r\right) \tag{14}$$

$T(\beta, n_1, n_2, L_R, r)$ is noted $\mathrm{T}(n_1.n_2)$ for sake of simplicity, with c the greatest common denominator between n_1 and n_2, $\varphi = \frac{360°}{n_1 n_2} c$, and, $\beta \in [0, \varphi_1]$. The number n_m is calculated with $n_{max} = \max(n_1, n_2)$ and $n_{min} = \min(n_1, n_2)$ the following process, illustrated in **Figure 3**,

- If

$$\frac{n_{max}}{n_{min}} = k \tag{15}$$

  with k an integer, then

$$n_m = \min\left(\frac{n_{min}}{c}, n_{max}\right) \tag{16}$$

  and,

$$\varphi_m = \min\left(\frac{360°}{n_{min}} \times c, \frac{360°}{n_{max}}\right) \tag{17}$$

- Else, if

$$\frac{n_{max}}{n_{min}} \neq k \tag{18}$$

  with k an integer and, with c' the greatest common denominator between n_{min} and $\frac{n_{max}}{c}$

  – If $c' \neq 1$, then

$$n_m = \min\left(\frac{n_{min}}{c}, n_{max}\right) \tag{19}$$

    and,

$$\varphi_m = \min\left(\frac{360°}{n_{min}} \times c, \frac{360°}{n_{max}}\right) \tag{20}$$

  – Else, if $c' = 1$, then

$$n_m = \min\left(n_{min}, \frac{n_{max}}{c}\right) \tag{21}$$

    and,

$$\varphi_m = \min\left(\frac{360°}{n_{min}}, \frac{360°}{n_{max}} \times c\right) \tag{22}$$

These conditions allow for the reduction of the contribution of the dipoles in a configuration, in c multiplied to the contribution of a base configuration. For instance, a configuration (3.6) with $c = 3$, and $6/3 = 2 = k$, the torque-angle contribution of (3.6) can be calculated as $T(, 3, 6) = 3 \times T(1, 6)$.

If a structure possesses m rings, the contribution of all the rings needs to be added. Each m ring possesses n_m dipoles with a distance r_m to the previous ring (with $r_1 = L_R$). The contribution of all m rings is calculated from **Equation 14** as

$$T_T(\beta, n_1, .., n_m, r_1, ..., r_m) = \sum_{i=1}^{m} \sum_{j=i+1}^{m} T(\beta, n_i, n_j, R_i, R_{ij}) \tag{23}$$

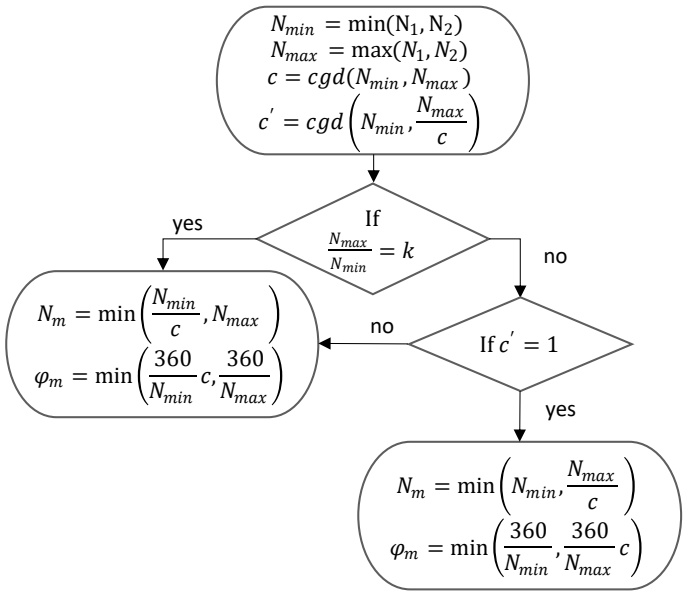

FIGURE 3: ILLUSTRATION OF THE FLOW CHART OF THE PROCESS FOR DEFINING n_m AND φ_m IN EQUATION 14 FOR A CONFIGURATION ($n_1.n_2$).

The distance between the center and ring r_i noted R_i is

$$R_i = \sum_{k=1}^{i} r_k \tag{24}$$

and the distance between two rings r_i and r_j is R_{ij}

$$R_i j = \sum_{i}^{j} r_i \tag{25}$$

The contribution to the torque-angle relation is dependent on the square of distances, the further the ring, the weaker its contribution.

For sake of simplicity the total Torque of any configuration (N_1,...,N_2) will be written $T(N_1.....N_2)$, for instance the torque of the configuration (3.4.7) is written $T(3.4.7)$.

The calculation of the torque-angle relation using the previous equations gives only negative values for attractive configurations ($Q < 0$) and only positive values for repulsive configurations ($Q > 0$). In order to obtain a torque-angle relation centered around $T = 0N.m$ the constant C_N is added to the **equations 5, 13, 14 and 23**, with C_N written as

$$C_N = \frac{1}{2}\left(T_{max} + T_{min}\right) \tag{26}$$

with T_{max} and T_{min} respectively the maximum and minimum values of the torque-angle relation. For attractive configurations $T_{max} = T(\varphi, n_1, n_2, L_R, r)$ and $T_{min} = T(0, n_1, n_2, L_R, r)$, inversely for repulsive configurations.

The factor Q could be tuned to modify the amplitude of the torque-angle, for instance to match the experimental and simulation data. In addition the model does yield to a minimal value at 0° for attractive configurations and a maximal value for repulsive configurations a phase shift ϕ could be applied for obtaining a model that starts at $0N.m$ at 0°.

2.3 Design of concentrical ring magnet-based multistable rotational stage

The torque-angle relation for magnet-based rotational multistable structure is highly dependent on the number of magnets or dipoles, the length of the moment arm and the distance between two rings, i.e. the position of the circles where the dipoles are located.

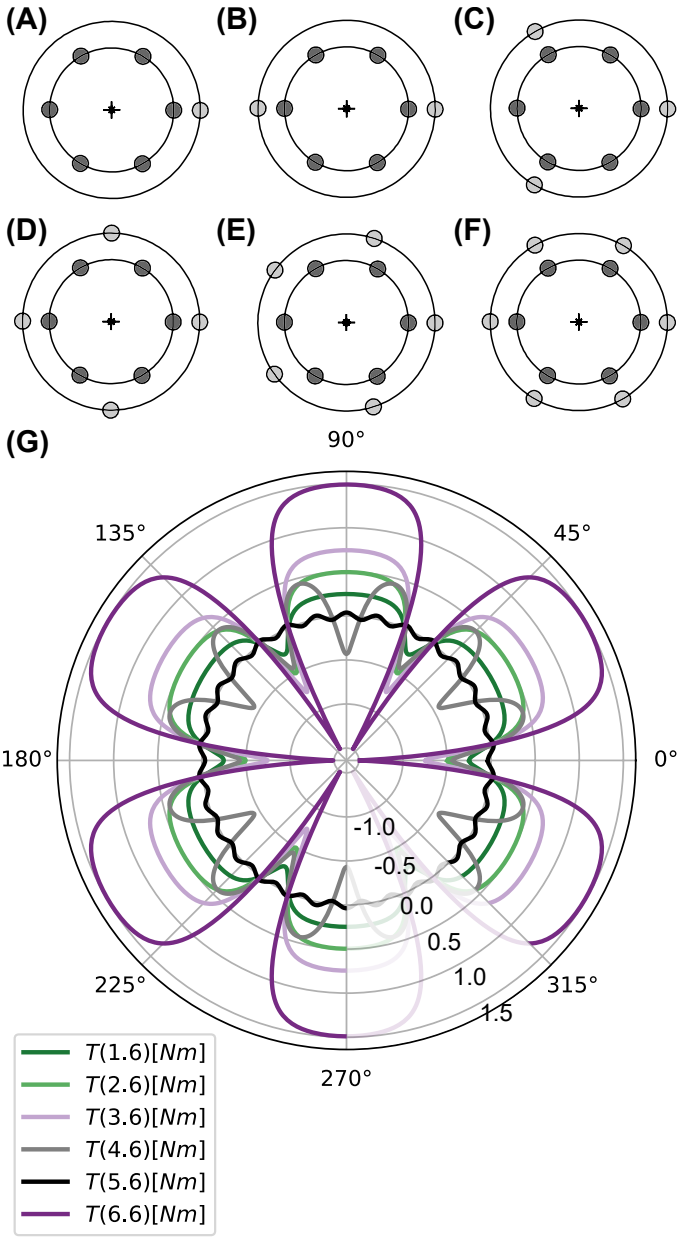

FIGURE 4: REPRESENTATION OF THE ATTRACTIVE CONFIGURATIONS (A) (1.6), (B) (2.6), (C) (3.6), (D) (4.6), (E) (5.6), (F) (6.6) AND (G) THE EVOLUTION OF THE TORQUE-ANGLE RELATION FOR THE ATTRACTIVE ($Q = -1.10^{-9} N.m^2$) CONFIGURATIONS (N.6) WITH $N = [1, 2, 3, 4, 5, 6]$ FOR $L_R = 49mm$ AND $R = 12mm$.

In addition, a minimum of three dipoles, and two rings are necessary to obtain multistability. It is possible to define the combinations of rings and dipoles using the prime factors of the number of desired stable states N. Two cases exist depending on N. First, if N is a prime number, only one decomposition exists with two rings, one of the ring possesses $n_1 = N$ dipoles and, the second possesses $n_2 = 1$ dipole. The angle between the N dipoles of the first ring is

$$\varphi_N = \frac{360°}{N} \tag{27}$$

Two permutations are possible for designing the structure, the inner ring can posses one dipole and the outer ring possesses $N = n_1$ dipoles, giving the configuration $(1.N)$, oppositely the inner ring possesses N dipoles and, the outer ring only one, yielding the configuration $(N.1)$. In this configuration, as there is only one dipole in one of the ring, the amplitude of the torque is limited to the contribution of one dipole and is dependent on the distances between center and the inner ring, and the distance between the two rings.

The torque-angle relation for a $(1.N)$ or $(N.1)$ configuration is given by **Equation 13**.

Second, if N is not a prime number, it is possible to decompose N in prime factors.

$$N = n_1 \times n_2 \times ... \times n_m \tag{28}$$

where N possesses m prime factors. The decomposition in prime factors enable to define the possible ring and dipole configurations. A number N of stable states can be configured into m rings, each ring possessing n_i dipoles (with $n_i \in [n_1, ..., n_m]$), forming an angle

$$\varphi_i = \frac{360°}{n_i} \tag{29}$$

There exist a number of p possible permutations of the m rings counted as

$$p = \frac{m!}{\prod_{i=2}^{m} r_i} \tag{30}$$

with r_i the number repetition of each prime factor. If f prime factors are combined, then $m!$ is replaced by $(m-j)$ in **Equation. 30**. The number M of dipoles is then defined as

$$M = \sum_{d=1}^{m} n_d \tag{31}$$

with n_d the number of dipoles per ring.

It is possible to combine two or more prime factors into one ring, leading to a ring possessing, for instance $N_1 = n_i \times n_j \times n_k$ dipoles, the angle between these dipoles is

$$\varphi_{ijk} = \frac{360°}{n_i n_j n_k} \tag{32}$$

These combinations allow for a control of the angle of rotation between two rings and the amplitude of the torque, where the minimal rotation angle between two rings $(n_1.n_2)$ is given as

$$\varphi_N = \frac{360°}{n_1 \times n_2} \times c \tag{33}$$

with c the greatest common divisor between n_1 and n_2. c is required to prevent for duplicates of angles to appear in the cases where rings are sharing the position of dipoles.

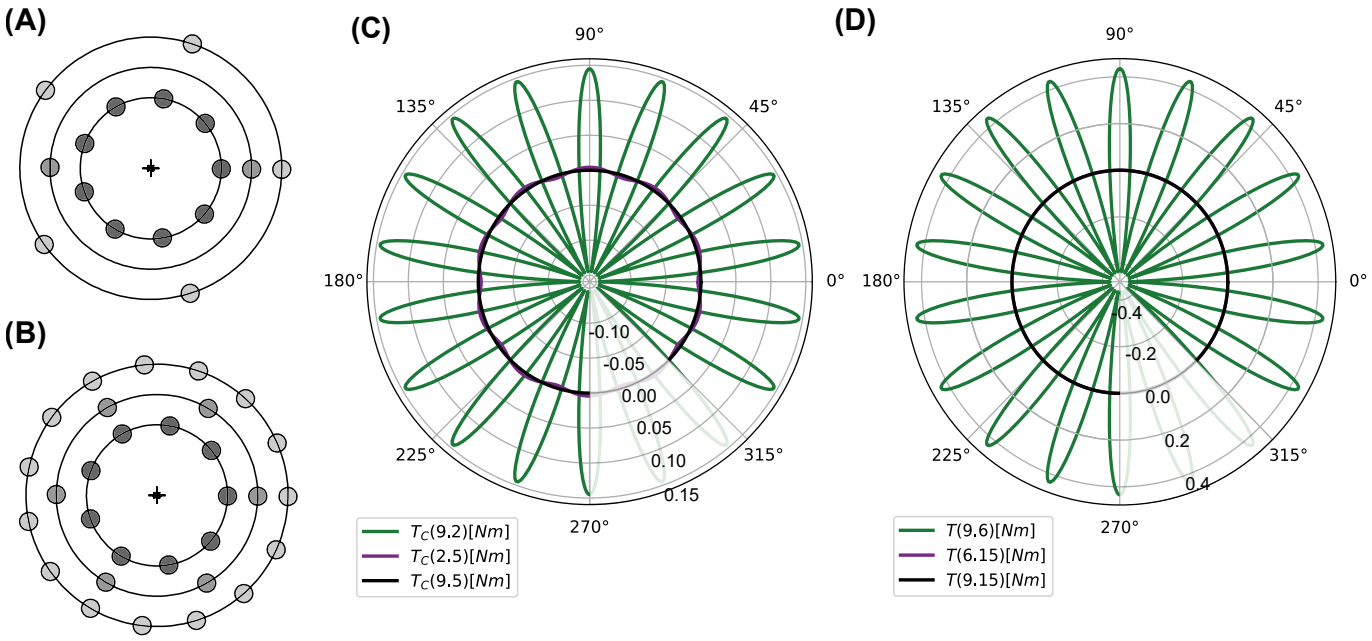

FIGURE 5: REPRESENTATION OF THE CONFIGURATIONS OF THE MULTISTABLE STRUCTURES (A) (9.2.5), (B) (9.6.15) AND THE EVOLUTION OF THE TORQUE-ANGLE RELATIONS FOR (C) (9.2.5) AND (D) (9.6.15) WITH $Q = -1.10^{-9} N.m^2$ AND DIMENSIONS $L_R = 49mm$ AND $r = 12mm$.

It is therefore possible to design the number of stable positions while finding the base configuration (N_1,N_2) and to design the stiffness by multiplying N_1 by the prime factors of N_2. For instance for the base configuration (1.6), with $N_1 = 1$ and $N_2 = 6$ has 6 stable positions and it is possible to increase the stiffness of the configuration by multiplying N_1 by the decomposition of the prime factors of $N_2 = 6 = 2 \times 3$, thus N_1 can be multiplied by $c \in C$ where C is the list of all possible products of the prime factors of N_2 and here $C = [2, 3, 6]$. Therefore, as a generalization, all the possible configurations that increase the stiffness from a base (N_1.N_2) are ($c \times N_1$.N_2).

For instance, the configurations (N.6) can be designed with $N \in [1, 6]$, illustrated in **Figure 4**. The torque-angle relation for the configuration (1.6) is given with **Equation 13** and possesses $N = 6$ stable positions. The determination of the relation for the configuration (2.6) follows the **Equation 14** with the selection process. In this case, the greatest common denominator $c = 2$, $n_m = 1$, $\varphi_m = 60°$ and $\varphi = 60°$, therefore the torque-angle relation T(2.6) = 2T(1.6). The same applies for T(3.6) = 3T(1.6) and T(6.6) = 6T(1.6), all these configurations possess also $N = 6$ stable positions.

However, the cases (4.6) and (5.6) are different. The configuration (4.6) has $c = 2$ and $6/4 \neq k$ and $c' = 1$, therefore $\varphi = 30°$ and T(4.6) = 2T(4.3), with $N = 12$ stable positions. And (5.6) has $c = 1$ thus has $\varphi = 12°$, with $N = 30$ stable positions, the torque-angle relations for the configurations (N.6) are plotted in **Figure 4.G**.

3. RESULTS

In this section, we propose to use design method for multistable rotating stage to design a stage that rotates of an angle $\varphi = 4°$ with a desired torque-angle relation. First, we use the theory to design the rings and the number of magnets per ring. Second, we simulate the behavior of the stage with a Finite Element Analysis (FEA). Third, we build the stage and experimentally validate the behavior.

3.1 Design of a multistable rotating stage

We aim in designing a multistable rotational stage that can position two concentrical hypothetical tools independently, with a high stiffness for the first tool and a lower stiffness for the second, with a total step angle of $\varphi = 4°$, using **Equation 27** we find $N = 90$ stable states. N can be decomposed in prime factors $90 = 2 \times 3 \times 3 \times 5$, the 3×3 needs to be combined to prevent modifying the angle φ, thus we select the three-ring configuration (9.2.5), illustrated in **Figure 5.A**. Indeed, if the 3×3 were not combined, it could result in a configuration (3.6.5) for instance where the contribution of (3.6) would result in an equivalent contribution of 3(1.6) with an angle $\varphi_{(3.6)} = 60°$ multiplying by three the angle of the configuration (9.2) with $\varphi_{(9.2)} = 20°$. We decided to use an attractive configuration for the realization of the prototype as the system was easier to assemble, therefore we will use $Q = -1.10^{-9} N.m^2$. The dimensions of the stage are $L_R = r_1 = 49mm$, $r_{12} = 12mm$, $r_{13} = 24.5mm$ and, $r_{23} = 12.5mm$ with the position of the dipoles taken as the center of the magnets of the multistable stage built in **Section 3.3**.

We observe in the torque-angle relation **Figure 5.C** that the contribution of (9.2) is significantly larger than the contribution of (2.5), the contribution of (9.5) separated between the middle ring is negligible.

To increase the contributions of (9.2) and (2.5) closer two options exist, the first would be to reduce the distance R_{12} between the inner and middle ring and, second to increase the number of dipoles in the middle and outer rings.

The model correctly indicates the values of the stable angles of the configurations however, the amplitude is uncertain and the factor Q might need to be adapted and possibly different for each configurations. The experimental and simulated results would enable to find a fit of the Q factor and the phase shift ϕ.

We decided to increase the number of dipoles because of spatial limitations, for instance. The second ring possessing $n_2 = 2$ dipoles brings the contribution of only two dipoles, we would like to increase the stiffness of that ring, therefore we decided to multiply by c the number of dipoles n_2 while keeping the same angle of stability. There are only two possible choices for c as it has to be a common denominator between $n_1 = 3 \times 3$ and $n_2' = cn_2$, then $c \in \{3, 9\}$. We selected $c = 3$ leading to a configuration (9.6.5). We apply the same process to the rings (6.5) where $c \in \{2, 3\}$ to bring the configuration (9.6.15), illustrated in **Figure 5.B**. The torque-angle relations for the configuration (9.6.15) are plotted in **Figure 5.D**. We observe that indeed the contribution of (9.2) has been multiplied by three as (9.6) similarly for (6.5) to (6.15). The gap between the two contribution assures that moving the outer ring ($n_3 = 15$) would not affect significantly the position of the middle ring ($n_2 = 6$).

3.2 Simulation of the behavior of the stage

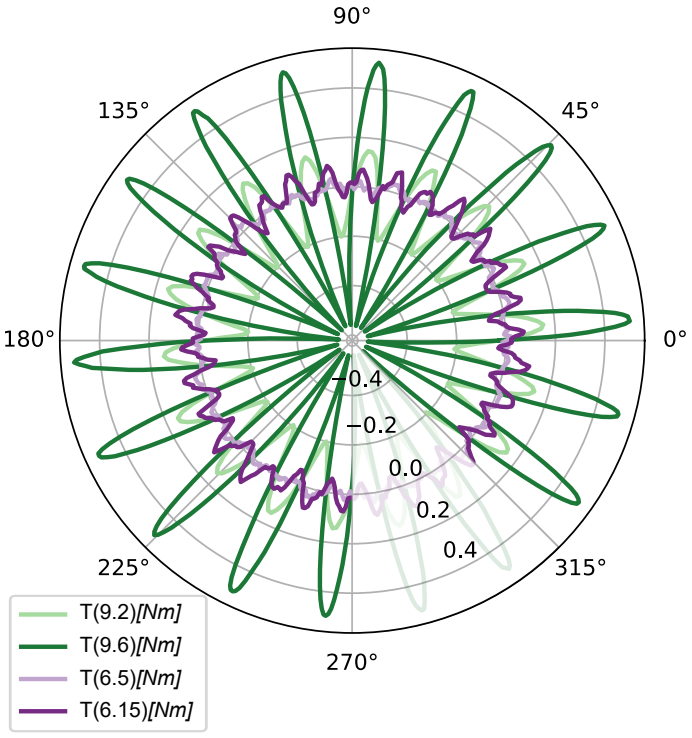

FIGURE 6: EVOLUTION OF THE SIMULATED TORQUE-ANGLE RELATIONS OF THE CONFIGURATIONS (9.2), (9.6), (6.5) AND (6.15).

The design method that we proposed in **Section 2.2.2** uses the ideal dipole assumption and uses Coulomb's law to define the multistable behavior of the stage. We used Comsol Multiphysics to simulate the behaviors of the configurations (9.2), (9.6), (6.5) and (6.15) with magnets (cube magnets of magnetization N45, holding force of 4.2kg and dimensions 10 x 10 x 10 mm) and using the dimensions given in **Section 3.1**. We used a recoil permeability $\mu_{rec} = 1.1$ and, a remanent flux density of $||\mathbf{B}_r|| = 1.35$T.

The torque-angle relations are plotted in **Figure 6**. The simulation show first a validation of the angle calculation for the configurations and validate the relation between a base configuration and the increase multiplication by c, for instance the amplitude of the torque-angle relation of T(9.6) is three times higher in amplitude than T(9.2), similarly for T(6.5) and T(6.15). Second, the simulations show that at $\beta = 0°$ the value of the torque is zero and have a similar stiffness in the two directions of rotation. The design method seems to capture the behavior of the torque-angle relation of T(9.2) and T(9.6) quite accurately however, struggles to capture the behavior of T(6.15) in terms of amplitude and therefore stiffness.

3.3 Experimental realization and validation of the behavior

To validate the results from the design method and the simulation we manufactured a stage with 90 stable states and a configuration (9.6.15) shown in **Figure 7.A**. The rings were 3D printed with PLA (polylactic acid) with a Prusa i3 MK3S. The inner ring has a diameter of 92 mm, and thickness of 12 mm, the middle ring has a diameter of 116 mm and a thickness on 12 mm and, the outer ring a diameter of 140 mm and a thickness of 13 mm. The rings are mounted on two ball bearings, between the inner and middle ring and, between the middle and outer ring. The magnets (Ni-Cu-Ni cube magnets of magnetization N45, holding force of 4.2kg and dimensions 10 x 10 x 10 mm, purchased from *www.magnetenspecialist.nl*) were inserted in the rings in an attractive configuration.

The multistable stage was fixed by the frame connection to the base of a tensile tester (Zwick Roell z005) and, the tensile tester connection of the stage was connected to the load cell, shown in **Appendix C**. The tensile tester measures the force and displacement of two subsystems. In the first configuration (9.6), the inner and middle rings are tested while the outer ring is fixed to the middle ring, in the second configuration (9.15), the inner and middle rings are fixed together, with both an angular displacement of 20°, at a speed of 60 mm/min.

The measured torque-angle results of the tensile tests are presented in **Figure 7.B**, in red for the configuration (6.15) and in black for (9.6). The experimental plots are superimposed to the simulation plots and show a great fit in the values of angles and the amplitude of the torque. The measured torque-angle of (9.6) seems to be shifted to the negative values but follows the simulated curve. The torque-angle of (6.15) follows the simulated plot very accurately between 0° and 20° however presents a dip in the negative angles. The experimental variations could be caused by the loading arm which does not stay vertical along the 40° of the experiment.

In addition, we superimposed the theoretical model for the configurations (9.6) and (6.15), the model predicted the correct angle of multistability, however, torque-angle relation were out of phase and a phase shift of $\phi_{(9.6)} = 5°$ and $\phi_{(6.15)} = 3°$ had to be applied, they correspond to $\phi = \varphi/4$. The amplitudes were not fitting, the factors Q had to be adapted and different to

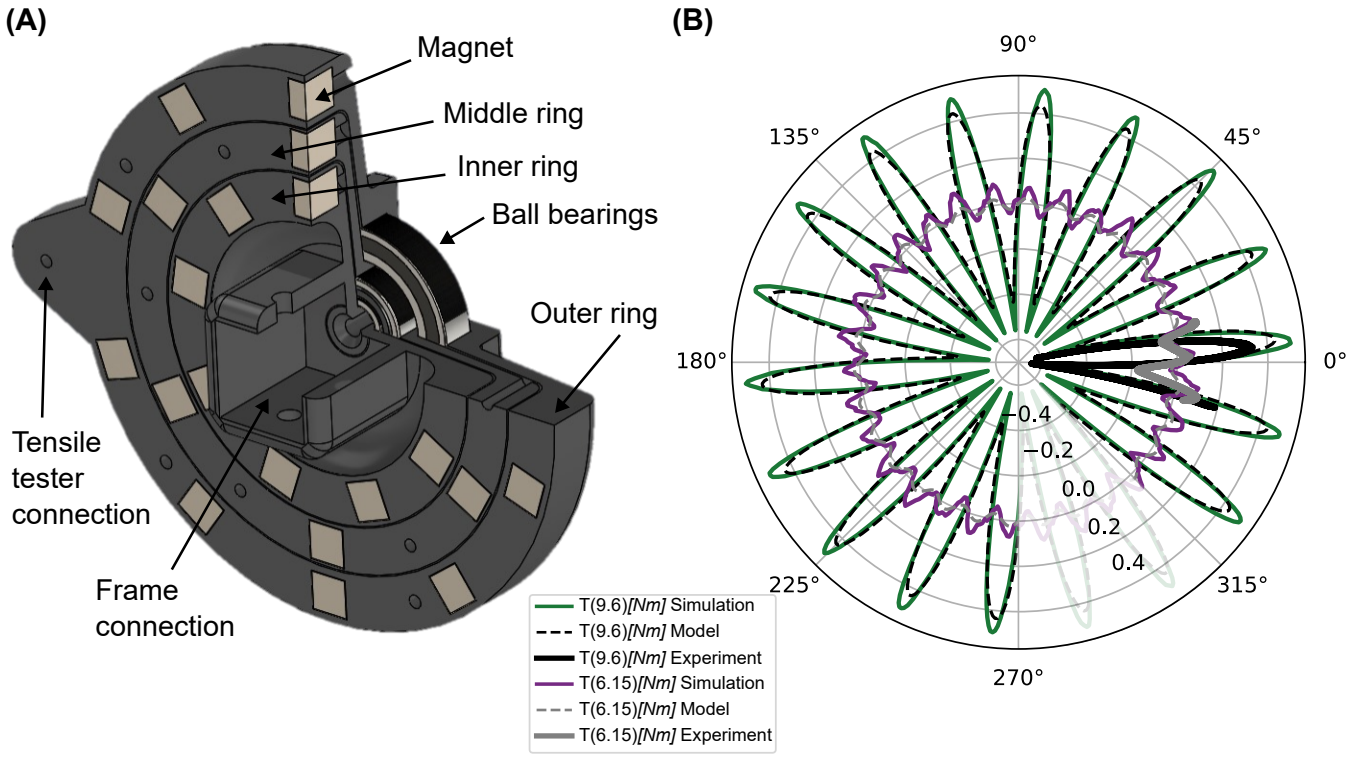

FIGURE 7: REPRESENTATION OF (A) THE MULTISTABLE STRUCTURE WITH THE CONFIGURATION (9.6.15) AND, (B) THE RESULT OF THE TENSILE TEST MEASUREMENTS ON TWO PAIRS OF RINGS (9.6) AND (6.15).

describe the model, with $Q_{(9.6)} = -1.10^{-8.95} N.m^2$ and $Q_{(6.15)} = -1.10^{-6.6} N.m^2$. These adaptations allow for a quite accurate fit of the model to simulations and experiments. We observe that for the (6.15) configuration, the experimental curve presents a dip, we suspect that this dip is caused because of the presence of the inner ring which impacts the torque-angle behavior of the middle to outer rings.

4. DISCUSSION

The proposed design method, based on the ideal dipole assumption, allow for the design of multi-ring magnet-based multistable rotational stages. Two types of output can result from the design method, first all the N stable states possess the same angle and stiffness. In this scenario, close to the design of magnetic motors, the ideal configuration seems to be a two-ring design $(N_1.N_2)$ where the $N = N_1 \times N_2$ states dictate the angle of rotational stability φ_N, the amplitude of the dips, related to stiffness, can be increased by multiplying the number of magnets N_1 by one or more prime factors of the decomposition of N_2 (respectively multiplying the number of magnets N_2 by one or more prime factors of the decomposition of N_1). The prime factor multiplication offers a limited amount of possibilities for modifying the stiffness, an other source of modification is the distance between the two rings.

Second, the N states do not have the same angle and stiffness. In this scenario we recommend to design a multi-ring stage, the decomposition of the N stable states in the prime factors and the possibility of combining the repeated factors prevent from reducing the number of states and thus increasing the angle. The stiffness of the rings could be design by their positions, the lowest stiffness is obtain by ordering the rings from the lowest number of magnet to the largest, in that case the torque-angle relations could be combined to design a specific envelop.

However, if the rings needs to be independent from each other configurations where the largest number of magnets are located at the center would be preferred. Additionally, these two behavior could be combined with an alternation of high and low number of magnets in order to reduce the stiffness difference, as we proposed with the (9.6.15) configuration.

A multi-ring configuration could be interesting to use in application that require the positioning of different elements with specific rotational stiffness and positioning angles. However, the actuation of a multi-ring stage would require the isolation of the ring intended to move from the others, in order to target a specific angle of rotation.

Our model is based on the electrostatic assumption to calculate the torque-angle relationships. This approximation provides a useful means of understanding the multistable angular behavior of a magnet-based multistable stage.

The electrostatic constant Q was initially assigned an arbitrary value of $Q = \pm 1 \cdot 10^{-9}\,\mathrm{N \cdot m^2}$. While this served as a starting point, the value of Q must be adjusted for each ring in a given configuration. However, a more thorough development of the electrostatic model is required to rigorously define and justify the value of Q.

The constant Q can be interpreted as an electrostatic analogue that may be physically related to the magnetic dipole interactions

between two magnets. Confirming this hypothesis would require extending the current electrostatic model into a magnetic model.

The phase shift ϕ is another parameter calibrated to match both experimental and simulation results for the configurations (9.6) and (6.15). For these cases, a value of $\phi = \varphi/4$ was found to provide a good fit, corresponding approximately to 5°. As with Q, a deeper development of the model is needed to establish a physical basis for ϕ.

Despite the model's utility, it faces limitations in accurately capturing low torque-angle behavior. For instance, the configuration (6.15) is not well represented by the current method. This suggests that an improved, magnet-based design methodology could yield more accurate results.

In summary, the electrostatic parameters Q and ϕ must be carefully adapted within the model. Establishing a clear link between these parameters and the magnetic properties of the system would enhance our understanding of the interactions and improve the accuracy of torque-angle predictions.

5. CONCLUSION

In summary, we have presented a design framework for the design of magnet-based multistable rotating structures. Our approach includes a mathematical design method based on the assumption of ideal dipoles and the use of Coulomb's law, we propose a calculation of the torque-angle relation using the contribution of all the dipoles in the system and calculate the stiffness associated. We applied this design framework to the design of a three-ring structure possessing 90 stable positions. The simulations and experimental measurements allow for a validation of our expectations given by the design method. Overall, our findings provide a valuable contribution in the field of multistability and can serve as a basis for the design and fabrication of magnet-based multistable structures.

ACKNOWLEDGMENTS

This publication is part of the project Mechanical Metamaterials for Compact Motion Systems (MECOMOS), project number 18940 of the Open Technology Program financed by the Dutch Research Council (NWO).

REFERENCES

[1] Meeussen, A. S. and van Hecke, M. "Multistable sheets with rewritable patterns for switchable shape-morphing." Vol. 621 No. 7979 (2023): pp. 516–520. DOI 10.1038/s41586-023-06353-5.

[2] Chi, Yinding, Li, Yanbin, Zhao, Yao, Hong, Yaoye, Tang, Yichao and Yin, Jie. "Bistable and Multistable Actuators for Soft Robots: Structures, Materials, and Functionalities." Vol. 34 No. 19 (2022): p. 2110384. DOI 10.1002/adma.202110384.

[3] Shahryari, Benyamin, Mofatteh, Hossein, Sargazi, Arian, Mirabolghasemi, Armin, Meger, David and Akbarzadeh, Abdolhamid. "Programmable Shape-Preserving Soft Robotics Arm via Multimodal Multistability." (2024): p. 2407651DOI 10.1002/adfm.202407651.

[4] Lakes, R.S. "Extreme damping in compliant composites with a negative-stiffness phase." Vol. 81 No. 2 (2002): pp. 95–100. DOI 10.1080/09500830010015332.

[5] Wu, Nan, Fu, Jiyang and Xiong, Chao. "A Bio-Inspired Bistable Piezoelectric Structure for Low-Frequency Energy Harvesting Applied to Reduce Stress Concentration." Vol. 14 No. 5 (2023): p. 909. DOI 10.3390/mi14050909.

[6] Qiu, J., Lang, J.H. and Slocum, A.H. "A Curved-Beam Bistable Mechanism." Vol. 13 No. 2 (2004): pp. 137–146. DOI 10.1109/JMEMS.2004.825308.

[7] Schioler, T. and Pellegrino, S. "Space Frames with Multiple Stable Configurations." Vol. 45 No. 7 (2007): pp. 1740–1747. DOI 10.2514/1.16825.

[8] Yang, Hang and Ma, Li. "Multi-stable mechanical metamaterials with shape-reconfiguration and zero Poisson's ratio." Vol. 152 (2018): pp. 181–190. DOI 10.1016/j.matdes.2018.04.064.

[9] Pan, Diankun, Wu, Zhangming, Dai, Fuhong and Tolou, Nima. "A novel design and manufacturing method for compliant bistable structure with dissipated energy feature." Vol. 196 (2020): p. 109081. DOI 10.1016/j.matdes.2020.109081.

[10] Rafsanjani, Ahmad, Akbarzadeh, Abdolhamid and Pasini, Damiano. "Snapping Mechanical Metamaterials under Tension." Vol. 27 No. 39 (2015): pp. 5931–5935. DOI 10.1002/adma.201502809.

[11] Tan, Xiaojun, Wang, Bing, Zhu, Shaowei, Chen, Shuai, Yao, Kaili, Xu, Peifei, Wu, Linzhi and Sun, Yuguo. "Novel multidirectional negative stiffness mechanical metamaterials." Vol. 29 No. 1 (2019): p. 015037. DOI 10.1088/1361-665X/ab47d9.

[12] Santer, Matthew and Pellegrino, Sergio. "Concept and Design of a Multistable Plate Structure." Vol. 133 No. 8 (2011). DOI 10.1115/1.4004459.

[13] Zhang, Yong, Wang, Qi, Tichem, Marcel and van Keulen, Fred. "Design and characterization of multistable mechanical metastructures with level and tilted stable configurations." Vol. 34 (2020): p. 100593. DOI 10.1016/j.eml.2019.100593.

[14] Jeong, Hoon Yeub, An, Soo-Chan, Seo, In Cheol, Lee, Eunseo, Ha, Sangho, Kim, Namhun and Jun, Young Chul. "3D printing of twisting and rotational bistable structures with tuning elements." Vol. 9 No. 1 (2019): p. 324. DOI 10.1038/s41598-018-36936-6.

[15] Pan, Diankun, Xu, Yulong, Li, Wenbing and Wu, Zhangming. "Novel rotational motion actuated beam-type multistable metastructures." Vol. 224 (2022): p. 111309. DOI 10.1016/j.matdes.2022.111309.

[16] Hewage, Trishan A. M., Alderson, Kim L., Alderson, Andrew and Scarpa, Fabrizio. "Double-Negative Mechanical Metamaterials Displaying Simultaneous Negative Stiffness and Negative Poisson's Ratio Properties." Vol. 28 No. 46 (2016): pp. 10323–10332. DOI 10.1002/adma.201603959.

[17] Tan, Xiaojun, Chen, Shuai, Wang, Bing, Zhu, Shaowei, Wu, Linzhi and Sun, Yuguo. "Design, fabrication, and characterization of multistable mechanical metamaterials

for trapping energy." Vol. 28 (2019): pp. 8–21. DOI 10.1016/j.eml.2019.02.002.

APPENDIX A. DERIVATION OF THE ROTATIONAL STIFFNESS $\kappa(\beta, L_R, r)$

The rotational stiffness is defined as the derivative of the torque in **Equation 10** as

$$\kappa(\beta, L_R, r) = \frac{dT(\beta, L_R, r)}{d\beta} \tag{34}$$

The function $T(\beta, L_R, r)$ is the fraction of two functions $f(\beta) = QL_R(L_R + r)\sin(\beta)$ and $g(\beta) = d^3(\beta) = h^{\frac{3}{2}}(\beta)$ with $h(\beta) = (L_R+r)^2+L_R^2-2L_R(L_R+r)\cos(\beta)$. The derivative of $T(\beta, L_R, r)$ can be written $T'(\beta)$ as

$$T'(\beta) = \frac{f'(\beta)g(\beta) - f(\beta)g'(\beta)}{g^2(\beta)} \tag{35}$$

with $f'(\beta) = QL_R(L_R + r)\cos(\beta)$ and $g^2(\beta) = d^6(\beta) = h^3(\beta)$. The calculation of the derivative $g'(\beta)$ can be calculated with the derivative of a function power n as

$$\frac{d(h(\beta))^{\frac{3}{2}}}{d\beta} = \frac{3\sqrt{h(\beta)}}{2}h'(\beta) \tag{36}$$

with $h'(\beta) = 2L_R(L_R + r)\sin(\beta)$ Therefore, the rotational stiffness can be written with the functions $f(\beta)$ and $h(\beta)$ as

$$\kappa(\beta) = \frac{f'(\beta)(h(\beta))^{\frac{3}{2}} - f(\beta)\frac{3\sqrt{h(\beta)}}{2}h'(\beta)}{h^3(\beta)} \tag{37}$$

APPENDIX B. IMPACT OF THE DIMENSIONS L_R AND r ON THE TORQUE-ANGLE RELATION

The torque-angle relation is dependent on the square of the dimensions L_R and R, therefore, a slight change in the dimensions changes significantly the values of the torque-angle as represented in **Figure 8**. When R is large enough compared to L_R then the torque-angle relation becomes almost a circle close to the value of $0Nm$ removing the multistability effect. Oppositely, bringing the rings closer, reducing the value of R, increases significantly the torque gap between two stable states.

APPENDIX C. EXPERIMENTAL SETUP

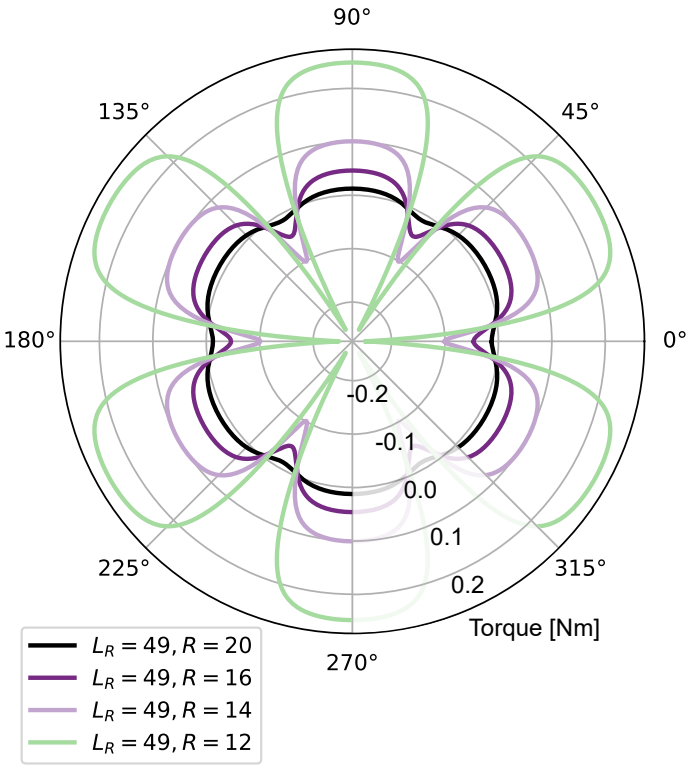

FIGURE 8: EVOLUTION OF THE TORQUE-ANGLE RELATION FOR THE ATTRACTIVE ($Q = -1.10^{-9}N.m^2$) CONFIGURATION (1.6) FOR THE DIMENSIONS $L_R = 49mm$ AND $R \in [12, 14, 16, 20]mm$.

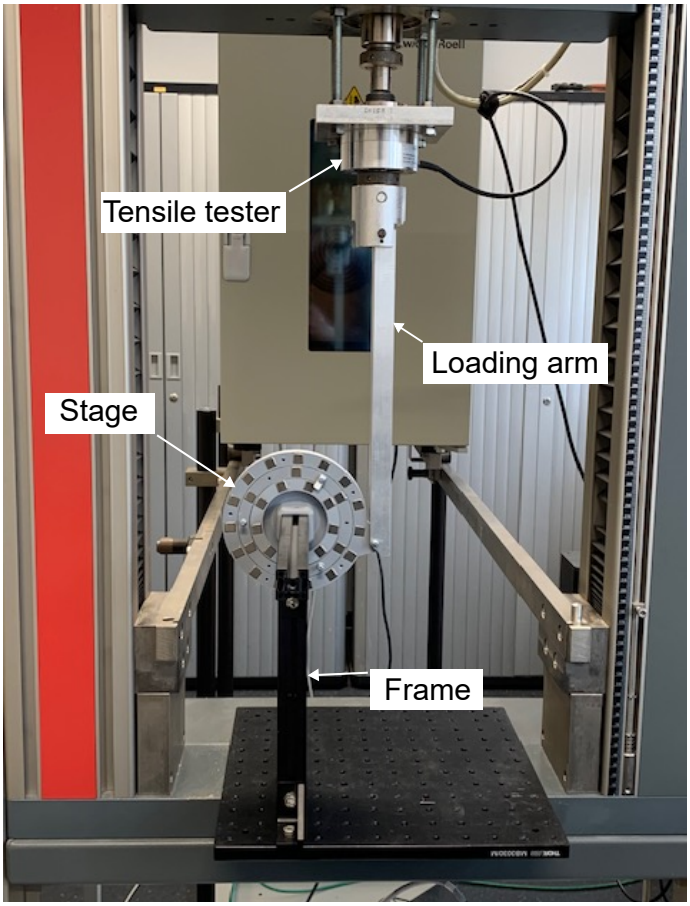

FIGURE 9: PHOTOGRAPHY OF THE EXPERIMENTAL SET UP WITH THE TENSILE TESTER ZWICK ROELL Z005 AND THE STAGE (9.6.15) MOUNTED ON THE FRAME AND CONNECTED TO THE LOADING ARM. THE MIDDLE RING COULD BE FIXED TO, EITHER THE INNER OUR OUTER RING TO COUPLE THEM.